Pseudo arrivals generated by frequency normalization for seismic interferometry with scattered waves ~ stationary-phase analysis ~

Nori Nakata[1], [1]*Massachusetts Institute of Technology, MA USA*

SUMMARY

Recent development of continuous recording systems used in industry, computational power, and very dense recording system makes seismic interferometry with ambient noise data an interesting tool to estimate structural information. To overcome the complexities of ambient noise, spectral normalization (e.g., whitening) is often used. Here I study different spectral normalization methods, such as crosscorrelation, deconvolution and crosscoherence, using numerical experiments and stationary-phase approximation. In the ideal situation of noise distribution, direct waves are accurately observed for all methods, but scattered waves are not. Especially, coda waves contain a lot of pseudo arrivals. Therefore, if we do not pay attention for the pseudo arrivals, we would use these waves for structural imaging and monitoring and create artifacts. Characterization of such waves using stationary-phase analyses sheds light on using and/or suppressing them.

INTRODUCTION

Seismic interferometry and ambient-noise correlation analyses have been used for Green's function retrieval, seismic tomography and time-lapse analyses (e.g., Wapenaar et al., 2010a,b). Most studies of tomography use fundamental-mode Rayleigh waves propagating directly from one receiver to the others (e.g., Shapiro et al., 2005). Love waves, higher-mode surface waves, and body waves have been also extracted from ambient noise and used for understanding the subsurface structure (Nakata et al., 2015; Czarny et al., 2019). For time-lapse analyses, due to the high sensitivity to the medium changes, multiply-scattered waves (e.g., coda waves) are often used, and one applies coda-wave interferometry to measure the subsurface velocity changes (Snieder et al., 2002; Brenguier et al., 2008). In addition, reflected waves are extracted at variety of scales (Ruigrok et al., 2008; Draganov et al., 2009; Nakata et al., 2011a; Girard and Shragge, 2020; Brenguier et al., 2019). Recent development of continuous recording systems used in industry, computational power, and very dense receiver arrays makes seismic interferometry with ambient noise data an interesting tool to map subsurface structure.

Theoretically, we can extract Green's functions between receivers by crosscorrelation (Wapenaar and Fokkema, 2006). Based on representation theorems, the assumptions we need to satisfy are energy equipartition of the ambient noise, far away sources from receivers or everywhere, and lossless media. As an ideal situation, I only consider the case, which holds these assumptions and will find the effects of frequency normalization. Because ambient noise is complex, we need to apply pre-processing to the continuously observed data. The pre-processing contains, for example, demean and detrend, stacking, spectral whitening, one-bit normalization, and removal of impulsive signals such as earthquakes. The idea of the pre-processing partly comes from the fact that the nature of the ambient noise does not satisfy the assumptions in the theoretical derivations. However, as I present here, spectral whitening and other frequency normalizations can general spurious multiples even under the ideal noise distribution.

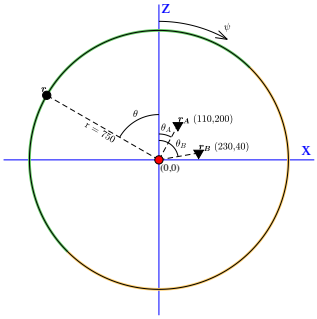

Figure 1: Geometry of source surface and receivers with convention of angles. The red dot shows the scatterer. The unit of the locations is meters. The green and yellow arcs are the source locations used for summation below.

Here, I first review different normalizations. I focus on crosscorrelation, deconvolution and spectral whitening (crosscoherence), but not one-bit normalization. We need statistical analyses for evaluating one-bit normalization, and for the sake of simplicity, I put this as a near-future topic. Next, I present a simple numerical example for problem statement. Then I use a stationary-phase approximation for different normalizations and discuss unphysical arrivals.

DEFINITION OF THREE NORMALIZATIONS

For ambient-noise correlation, I discuss three different frequency normalization techniques throughout this study: crosscorrelation, deconvolution and crosscoherence. To focus on the effect of the normalization, I assume that the noise sources are uniformly distributed, uncorrelated, and far from receivers. Let us consider $u(\mathbf{r}_A, \mathbf{r})$ and $u(\mathbf{r}_B, \mathbf{r})$ as frequency-domain wavefields excited at location $\mathbf{r}$ and recorded at locations $\mathbf{r}_A$ and $\mathbf{r}_B$, respectively. The locations are defined as

$$\mathbf{r}_{A,B} = \begin{pmatrix} x_{A,B} \\ 0 \\ z_{A,B} \end{pmatrix} = r_{A,B} \begin{pmatrix} \sin\theta_{A,B} \\ 0 \\ \cos\theta_{A,B} \end{pmatrix}, \quad \mathbf{r} = \begin{pmatrix} x \\ y \\ z \end{pmatrix} = r \begin{pmatrix} \sin\theta\cos\psi \\ \sin\theta\sin\psi \\ \cos\theta \end{pmatrix}$$

in the spherical coordinate (Figure 1). Crosscorrelation (CC) in the frequency domain is given by

$$CC = \left\{ \sum_{S} u(\mathbf{r}_A, \mathbf{r}) \right\} \left\{ \sum_{S'} u(\mathbf{r}_B, \mathbf{r}') \right\}^{*}, \tag{1}$$

where $*$ is the complex conjugate. When we assume that the phases of the noise sources are random and their source time

Table 1: Comparison of the terms in equations 7–9. The Phase and Term ID columns show the phase of each term and sequential term numbers.

Phase	Term ID	xcor	decon	coher
$G_{A0}G^*_{B0}$	$\mathcal{T}_1$	$\mathcal{CC}_1$	$\mathcal{DE}_1$	$\mathcal{CH}_1$
$G_{AS}G^*_{B0}$	$\mathcal{T}_2$	$\mathcal{CC}_2$	$\mathcal{DE}_2$	$\mathcal{CH}_2$
$G_{A0}G^*_{BS}$	$\mathcal{T}_3 = \mathcal{T}^*_2\vert_{A\leftrightarrow B}$	$\mathcal{CC}_3$		$\mathcal{CH}_3$
$G_{AS}G^*_{BS}$	$\mathcal{T}_4$	$\mathcal{CC}_4$		$\mathcal{CH}_4$
$G_{A0}G_{BS}(G^*_{B0})^2$	$\mathcal{T}_5$		$\mathcal{DE}_5$	$\mathcal{CH}_5$
$(G_{A0})^2G^*_{AS}G^*_{B0}$	$\mathcal{T}_6 = \mathcal{T}^*_5\vert_{A\leftrightarrow B}$			$\mathcal{CH}_6$
$G_{AS}G_{BS}(G^*_{B0})^2$	$\mathcal{T}_7$		$\mathcal{DE}_7$	$\mathcal{CH}_7$
$(G_{A0})^2G^*_{AS}G^*_{BS}$	$\mathcal{T}_8 = \mathcal{T}^*_7\vert_{A\leftrightarrow B}$			$\mathcal{CH}_8$
$G_{A0}G_{B0}(G^*_{BS})^2$	$\mathcal{T}_9$			$\mathcal{CH}_9$
$(G_{AS})^2G^*_{A0}G^*_{B0}$	$\mathcal{T}_{10} = \mathcal{T}^*_9\vert_{A\leftrightarrow B}$			$\mathcal{CH}_{10}$
$G_{A0}(G_{BS})^2(G^*_{B0})^3$	$\mathcal{T}_{11}$		$\mathcal{DE}_{11}$	$\mathcal{CH}_{11}$
$(G_{A0})^3G^*_{B0}(G^*_{AS})^2$	$\mathcal{T}_{12} = \mathcal{T}^*_{11}\vert_{A\leftrightarrow B}$			$\mathcal{CH}_{12}$
$(G_{A0})^2G_{BS}(G^*_{B0})^2G^*_{AS}$	$\mathcal{T}_{13}$			$\mathcal{CH}_{13}$

$\mathcal{T}_j = \mathcal{T}^*_i\vert_{A\leftrightarrow B}$ means that $\mathcal{T}_j$ is equal to the complex conjugate of $\mathcal{T}_i$ with exchanging receivers A and B.

functions are uncorrelated, equation 1 simplifies

$$CC = \sum_S u(\mathbf{r}_A,\mathbf{r})u^*(\mathbf{r}_B,\mathbf{r}). \tag{2}$$

This is a strong assumption but satisfied reasonably well if observation is long enough (Snieder, 2004). When the sources are densely and uniformly distributed at a surface dS, the summation over the sources can be replaced by an integration and equation 3 becomes

$$CC = n\oint u(\mathbf{r}_A,\mathbf{r})u^*(\mathbf{r}_B,\mathbf{r})dS = nr^2\oint u(\mathbf{r}_A,\mathbf{r})u^*(\mathbf{r}_B,\mathbf{r})d\Omega, \tag{3}$$

where n is the number of sources per unit surface area. For the last equal, I further assume the source distribution is at a sphere and conver the surface integral into the angle integral. Similarly, deconvolution ($\mathcal{DE}$), and crosscoherence ($\mathcal{CH}$) are given by

$$\mathcal{DE} = nr^2\oint \frac{u(\mathbf{r}_A,\mathbf{r})}{u(\mathbf{r}_B,\mathbf{r})}d\Omega = nr^2\oint \frac{u(\mathbf{r}_A,\mathbf{r})u^*(\mathbf{r}_B,\mathbf{r})}{|u(\mathbf{r}_B,\mathbf{r})|^2}d\Omega \tag{4}$$

$$\mathcal{CH} = nr^2\oint \frac{u(\mathbf{r}_A,\mathbf{r})u^*(\mathbf{r}_B,\mathbf{r})}{|u(\mathbf{r}_A,\mathbf{r})||u(\mathbf{r}_B,\mathbf{r})|}d\Omega, \tag{5}$$

respectively (Nakata et al., 2011b). Because the denominators for deconvolution and crosscoherence contain only amplitude information, and the numerators are the same as the term of crosscorrelation, the differences between these computations can be considered as different frequency normalization strategies. Therefore, the phases for these three techniques are identical. Interestingly, these differences in the amplitude modulate our signals and generate pseudo arrivals.

Decomposition of unperturbed and scattered waves

In general, the wavefield contains both unperturbed (direct; G_0) and scattered (G_S) Green's functions as

$$u(\mathbf{r}_A,\mathbf{r}) = W(\mathbf{r})\{G_0(\mathbf{r}_A,\mathbf{r}) + G_S(\mathbf{r}_A,\mathbf{r})\}, \tag{6}$$

for receiver A and similar for receiver B. In equation 6, $W(\mathbf{r})$ is a source function. For brevity, I use the simple notation below and rewrite equation 6 as $u_A = W(G_{A0} + G_{AS})$. Inserting equation 6 into equations 3–5, I obtain

$$CC = nr^2\oint |W|^2\left(\underbrace{G_{A0}G^*_{B0}}_{CC_1} + \underbrace{G_{AS}G^*_{B0}}_{CC_2} + \underbrace{G_{A0}G^*_{BS}}_{CC_3} + \underbrace{G_{AS}G^*_{BS}}_{CC_4}\right)d\Omega \tag{7}$$

$$\mathcal{DE} = nr^2\oint\left(\underbrace{\frac{G_{A0}G^*_{B0}}{|G_{B0}|^2}}_{\mathcal{DE}_1} + \underbrace{\frac{G_{AS}G^*_{B0}}{|G_{B0}|^2}}_{\mathcal{DE}_2} - \underbrace{\frac{G_{A0}G_{BS}(G^*_{B0})^2}{|G_{B0}|^4}}_{\mathcal{DE}_5} - \underbrace{\frac{G_{AS}G_{BS}(G^*_{B0})^2}{|G_{B0}|^4}}_{\mathcal{DE}_7} + \underbrace{\frac{G_{A0}(G_{BS})^2(G^*_{B0})^3}{|G_{B0}|^6}}_{\mathcal{DE}_{11}}\right)d\Omega \tag{8}$$

$$\begin{aligned}\mathcal{CH} = nr^2\oint\Bigg\{&\underbrace{\left(1 - \frac{1}{4}\frac{|G_{AS}|^2}{|G_{A0}|^2} - \frac{1}{4}\frac{|G_{BS}|^2}{|G_{B0}|^2}\right)\frac{G_{A0}G^*_{B0}}{|G_{A0}||G_{B0}|}}_{\mathcal{CH}_1} + \underbrace{\frac{1}{2}\frac{G_{AS}G^*_{B0}}{|G_{A0}||G_{B0}|}}_{\mathcal{CH}_2} + \underbrace{\frac{1}{2}\frac{G_{A0}G^*_{BS}}{|G_{A0}||G_{B0}|}}_{\mathcal{CH}_3}\\ &+ \underbrace{\frac{1}{4}\frac{G_{AS}G^*_{BS}}{|G_{A0}||G_{B0}|}}_{\mathcal{CH}_4} - \underbrace{\frac{1}{2}\frac{G_{A0}G_{BS}(G^*_{B0})^2}{|G_{A0}||G_{B0}|^3}}_{\mathcal{CH}_5} - \underbrace{\frac{1}{2}\frac{(G_{A0})^2G^*_{AS}G^*_{B0}}{|G_{A0}|^3|G_{B0}|}}_{\mathcal{CH}_6}\\ &- \underbrace{\frac{1}{4}\frac{G_{AS}G_{BS}(G^*_{B0})^2}{|G_{A0}||G_{B0}|^3}}_{\mathcal{CH}_7} - \underbrace{\frac{1}{4}\frac{(G_{A0})^2G^*_{AS}G^*_{BS}}{|G_{A0}|^3|G_{B0}|}}_{\mathcal{CH}_8} - \underbrace{\frac{1}{8}\frac{G_{A0}G_{B0}(G^*_{BS})^2}{|G_{A0}||G_{B0}|^3}}_{\mathcal{CH}_9} - \underbrace{\frac{1}{8}\frac{(G_{AS})^2G^*_{A0}G^*_{B0}}{|G_{A0}|^3|G_{B0}|}}_{\mathcal{CH}_{10}}\\ &+ \underbrace{\frac{3}{8}\frac{G_{A0}(G_{BS})^2(G^*_{B0})^3}{|G_{A0}||G_{B0}|^5}}_{\mathcal{CH}_{11}} + \underbrace{\frac{3}{8}\frac{(G_{A0})^3G^*_{B0}(G^*_{AS})^2}{|G_{A0}|^5|G_{B0}|}}_{\mathcal{CH}_{12}} + \underbrace{\frac{1}{4}\frac{(G_{A0})^2G_{BS}(G^*_{B0})^2G^*_{AS}}{|G_{A0}|^3|G_{B0}|^3}}_{\mathcal{CH}_{13}}\Bigg\}d\Omega,\end{aligned} \tag{9}$$

where I use Taylor expansions for deconvolution and crosscoherence similar to equations 3 and 15 in Nakata et al. (2013) and show up to the second-order scattered terms. Note that the source term W is canceled for deconvolution and crosscoherence as discussed in Nakata et al. (2011a). Based on Table 1, in terms of the phase, equations 7–9 have total 13 unique terms and crosscoherence contains all of them.

NUMERICAL EXPERIMENT

I first use a finite-difference wavefield modeling to visualize the effects of different normalization defined in equations 3–5. The source-receiver geometries are defined in Figure 1. In the numerical simulation, total 720 sources are located along the circle with a radius of 750 m with an even spacing and excited individually to satisfy the condition of no correlation between different sources. This is an ideal situation for seismic interferometry to extract the Green's function between receivers as demonstrated below. For the source function, I use the Ricker wavelet with central frequency of 50 Hz. The calculation area is sufficiently large (-1750 – 1750 m) with additional 300-m absorbing boundaries on each side to avoid having numerical reflected waves. I apply seismic interferometry with different normalization (equations 3–5) to the synthetic data. I also model the wave propagation from receiver B to receiver A to check interferometry results.

As expected, I can extract accurate Green's function for both direct and scattered waves using crosscorrelation (Figure 2a,d). Signals around -0.1 s on the green and yellow arcs (highlighted by CC_4) are canceled each other because of the generalized op-

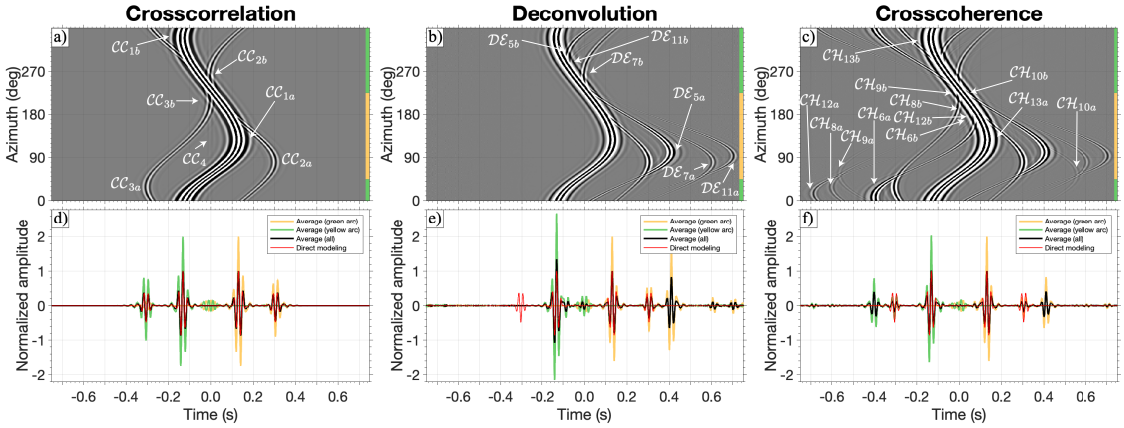

Figure 2: Wavefields after applying seismic interferometry: (a) crosscorrelation (equation 3), (b) deconvolution (equation 4), and (c) crosscoherence (equation 5). The amplitudes are clipped independently in each panel. Also an amplitude gain according to the square of time is applied to enhance the small signals in later time. Stationary phases for the terms in Table 1 are highlighted by white arrows. The green and yellow bars illustrate the location of sources shown in Figure 1. (d–f) Summation of wavefields over sources for crosscorrelation, deconvolution, and crosscoherence, respectively. For black, green and yellow lines, all sources, sources on the green arc in Figure 1, and sources on the yellow arc are used, respectively. The red line shows the wavefield modeled by the case when we put a source at the location of receiver B and record at receiver A. Amplitudes are normalized to make the signal at 0.15 s as 1, and the same amplitude gain according to the time as the upper-row panels is applied.

tical theorem (Snieder et al., 2008). Deconvolution interferometry, however, has no scattered waves in the negative time and creates several pseudo (and unphysical) arrivals in later time (Figure 2b,e). Similarly, crosscoherence interferometry produces pseudo arrivals as well (Figure 2c,f), although the amplitudes of such arrivals compared to direct waves are smaller than those in the deconvolved interferometry. Because the amplitude of scattered waves in crosscoherence is also smaller than the direct modeling, this normalization is efficient for extracting direct waves, but not scattered waves. Because of such pseudo arrivals, coda waves after seismic interferometry with spectral normalization contain unphysical waves. In the next section, with stationary-phase analyses, I will characterize each phase in Figure 2, which would be useful for avoiding to misinterpret such waves and designing filters to remove them.

STATIONARY-PHASE ANALYSIS

Following Snieder et al. (2008), I use stationary-phase approximations to solve equations 7–9. When we have a scatterer at the origin $(0,0)$, the total 3D acoustic-wave Green's function from point $\mathbf{r}$ to $\mathbf{r}_A$ can be defined as

$$G_{\rm tot}(\mathbf{r}_A,\mathbf{r}) = G_0(\mathbf{r}_A,\mathbf{r}) + G_S(\mathbf{r}_A,\mathbf{r}) = -\frac{\rho}{4\pi}\frac{\exp(ik|\mathbf{r}-\mathbf{r}_A|)}{|\mathbf{r}-\mathbf{r}_A|} - \frac{\rho}{4\pi}\frac{\exp(ikr)}{r} f(\hat{\mathbf{r}_A},-\hat{\mathbf{r}})\frac{\exp(ikr_A)}{r_A}, \tag{10}$$

where $\hat{\ }$ represents the wave direction and $f(\hat{\mathbf{r}_A},-\hat{\mathbf{r}})$ is the scattering coefficient for the wave propagating from $-\hat{\mathbf{r}}$ to $\hat{\mathbf{r}_A}$. Based on the derivation in Wapenaar and Fokkema (2006) and approximation in their equation 30, I employ the condition that sources are far from the receivers ($r \gg r_{A,B}$). For brevity, I consider the receivers which are at $x_A < x_B$ and $z_A > z_B$. Because we already understand the effect of the source wavelet W in the previous section, in the rest of this section, I assume $W = 1$, which is a delta function in the time domain, and $u(\mathbf{r}_A,\mathbf{r}) = G_{\rm tot}(\mathbf{r}_A,\mathbf{r})$.

Crosscorrelation

The stationary-phase approximation of crosscorrelation (equation 7) has been discussed by Snieder et al. (2008) and Halliday and Curtis (2009), and summarized by Nakata (2020). After inserting equation 10 into equation 7, the crosscorrelation becomes

$$CC = \frac{in\rho}{2k}\left\{\underbrace{G_0(\mathbf{r}_A,\mathbf{r}_B)}_{CC_{1a}} - \underbrace{G_0^*(\mathbf{r}_B,\mathbf{r}_A)}_{CC_{1b}} + \underbrace{G_s(\mathbf{r}_A,\mathbf{r}_B)}_{CC_{2a}} - \underbrace{G_s^*(\mathbf{r}_B,\mathbf{r}_A)}_{CC_{3a}}\right\} + \frac{n\rho^2\exp[ik(r_A-r_B)]}{4\pi k r_A r_B}\left[\frac{i}{2}\left\{\underbrace{f(\hat{\mathbf{r}_A},-\hat{\mathbf{r}_B})}_{CC_{2b}} - \underbrace{f^*(\hat{\mathbf{r}_B},-\hat{\mathbf{r}_A})}_{CC_{3b}}\right\} + \underbrace{\frac{k}{4\pi}\oint f(\hat{\mathbf{r}_A},-\hat{\mathbf{r}})f^*(\hat{\mathbf{r}_B},-\hat{\mathbf{r}})d\Omega}_{CC_4}\right], \tag{11}$$

where the subscripts a and b in each term indicate the stationary points at $\psi = 0$ and $\psi = \pi$, respectively. Due to the generalized optical theorem, terms in the square bracket are canceled (Snieder et al., 2008) (i.e., $CC_{2b} + CC_{3b} = CC_4$).

Deconvolution

For the stationary-phase approximation to deconvolution interferometry, I insert equation 10 into equation 8. Based on Table 1, Terms $\mathcal{DE}_5$, $\mathcal{DE}_7$, and $\mathcal{DE}_{11}$ are unique compared to crosscorrelation and these terms are related to the pseudo arrivals in Figure 2be. I demonstrate here the stationary-phase analysis for term $\mathcal{DE}_5$, and the analyses for other terms are shown by Nakata (2020).

Using equation 10, $\mathcal{DE}_5$ becomes

$$\mathcal{DE}_5 = -\oint \frac{r|\mathbf{r}-\mathbf{r}_B|^2}{r_B|\mathbf{r}-\mathbf{r}_A|} f(\hat{\mathbf{r}_B},-\hat{\mathbf{r}})\exp(ikL_5)d\Omega, \tag{12}$$

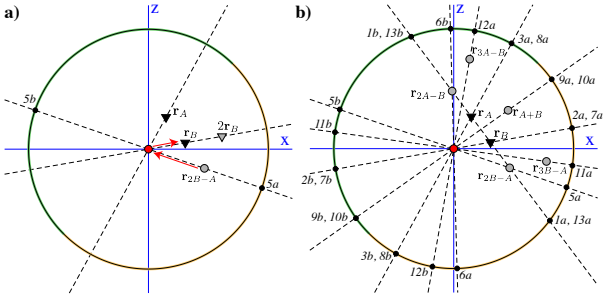

Figure 3: (a) The wave propagation of $\mathcal{DE}_5$ at the stationary point. The black points ($5a$ and $5b$) illustrate the location of stationary points. The red arrows indicate the ray path of the wave. (b) Stationary-phase points (black dots) for all terms shown in Table 1. The numbers next to the black dots show the term ID, and a and b denote the two stationary points for each term ($\psi = 0$ and π).

where

$$L_5 = (2x_B - x_A)\cos\theta\sin\theta + (2z_B - z_A)\cos\theta + r_B.$$

At the stationary phase (ψ_s, θ_s), the first derivatives of L_5 should be zero, and hence

$$\frac{\partial L_5}{\partial \psi} = -(2x_B - x_A)\sin\psi_s \sin\theta_s = 0 \tag{13}$$

$$\frac{\partial L_5}{\partial \theta} = (2x_B - x_A)\cos\psi_s \cos\theta_s - (2z_B - z_A)\sin\theta_s = 0. \tag{14}$$

From equation 13, two stationary phases exist at $\psi_{sa} = 0$ and $\psi_{sb} = \pi$. I first consider $\psi_{sa} = 0$, and with equation 14, I obtain $\tan\theta_{sa} = (2x_B - x_A)/(2z_B - z_A)$, which indicates that the angle of the stationary phase is not equal to the angle of either receivers A or B, which are the case for Terms $\mathcal{T}_2$ and $\mathcal{T}_3$, but the angle is related to the location of $2\mathbf{r}_B - \mathbf{r}_A$. We define $\mathbf{r}_{2B-A} = 2\mathbf{r}_B - \mathbf{r}_A$, and r_{2B-A} for its distance. At this stationary point, $L_5 = r_{2B-A} + r_B$, $\hat{\mathbf{r}} = \hat{\mathbf{r}}_{2B-A}$. For the stationary-phase analysis, we also need the second derivatives of L_5;

$$\frac{\partial^2 L_5}{\partial \psi^2} = -(2x_B - x_A)\sin\theta_s < 0$$

$$\frac{\partial^2 L_5}{\partial \theta^2} = -r_{2B-A} < 0. \tag{15}$$

Using equations 13–15 with the stationary-phase approximation, equation 12 becomes

$$\mathcal{DE}_{5a} = \frac{2\pi i r|\mathbf{r} - \mathbf{r}_B|^2}{k|\mathbf{r} - \mathbf{r}_A|} f(\hat{\mathbf{r}_B}, -\hat{\mathbf{r}}_{2B-A}) \frac{\exp(ik(r_{2B-A} + r_B))}{r_B r_{2B-A}}, \tag{16}$$

and similarly for the other stationary-phase point ($\psi_{sb} = \pi$),

$$\mathcal{DE}_{5b} = -\frac{2\pi i r|\mathbf{r} - \mathbf{r}_B|^2}{k|\mathbf{r} - \mathbf{r}_A|} f(\hat{\mathbf{r}_B}, \hat{\mathbf{r}}_{2B-A}) \frac{\exp(ik(-r_{2B-A} + r_B))}{r_B r_{2B-A}}. \tag{17}$$

This stationary-phase approximation reveals that the wavefield $\mathcal{DE}_5$ has a longer ray path, and the stationary point is aligned with the origin and points $\mathbf{r}_{2B-A}$ (Figure 3a).

Based on the concept of the clamped boundary condition for deconvolution interferometry (Snieder and Şafak, 2006; Vasconcelos and Snieder, 2008; Nakata et al., 2013), the wavefield $\mathcal{DE}_{5a}$ can be considered as the wave propagating from receiver B to the scatterer, scattered back to r_B, and then scattered again at r_B to propagate to receiver A because of the change in the boundary condition at r_B. The distance of the ray path for this wave is $2r_B + |\mathbf{r}_B - \mathbf{r}_A| \equiv r'$, which is different from L_5 at the stationary phase. When the scatterer, r_A, and r_B are aligning linearly (e.g., 1D wave propagation), L_5 and wave $\mathcal{DE}_{5a}$ at the stationary phase can be interpreted as the clamped boundary wave. However in general, $\mathcal{DE}_{5a}$ is equivalent to the wave where we artificially put a receiver at $\mathbf{r}_{2B-A}$ (Figure 3a).

When I solve terms $\mathcal{DE}_7$ and $\mathcal{DE}_{11}$ in with a stationary phase approximation, equation 8 becomes

$$\begin{aligned}\mathcal{DE} = N\Bigg[&\frac{2\pi i}{\rho k} G_0(r_A, r_B) - \frac{2\pi i}{\rho k} G_0^*(r_B, r_A) \\ &+ \frac{2\pi i}{\rho k} G_s(r_A, r_B) + \frac{i}{2k} f(\hat{\mathbf{r}_A}, \hat{\mathbf{r}_B}) \frac{\exp(ik(r_A - r_B))}{r_A r_B} \\ &+ \frac{i}{2k} f(\hat{\mathbf{r}_B}, -\hat{\mathbf{r}_{2B-A}}) \frac{\exp(ik(r_{2B-A} + r_B))}{r_B r_{2B-A}} - \frac{i}{2k} f(\hat{\mathbf{r}_B}, \hat{\mathbf{r}_{2B-A}}) \frac{\exp(ik(-r_{2B-A} + r_B))}{r_B r_{2B-A}} \\ &+ \frac{i}{4kr_B} f(\hat{\mathbf{r}_A}, -\hat{\mathbf{r}_B}) f(\hat{\mathbf{r}_B}, -\hat{\mathbf{r}_B}) \frac{\exp(ik(3r_B + r_A))}{r_A r_B} - \frac{i}{4kr_B} f(\hat{\mathbf{r}_A}, \hat{\mathbf{r}_B}) f(\hat{\mathbf{r}_B}, \hat{\mathbf{r}_B}) \frac{\exp(ik(r_A - r_B))}{r_A r_B} \\ &- \frac{i}{2kr_B} f^2(\hat{\mathbf{r}_B}, -\hat{\mathbf{r}_{3B-A}}) \frac{\exp(ik(r_{3B-A} + 2r_B))}{r_B r_{3B-A}} + \frac{i}{2kr_B} f^2(\hat{\mathbf{r}_B}, \hat{\mathbf{r}_{3B-A}}) \frac{\exp(ik(-r_{3B-A} + 2r_B))}{r_B r_{3B-A}}\Bigg],\end{aligned} \tag{18}$$

where N is the total number of sources ($N = 4\pi n r^2$). Note that because the deconvolution interferometry does not have term $\mathcal{T}_3$, the wave of $\mathcal{DE}_{2b}$ is not canceled and shown as a pseudo wave around -0.1 s in Figure 2e.

Crosscoherence

Next, I insert equation 10 into equation 9 and use the stationary-phase approximation to solve each term in Table 1. After the approximation, crosscoherence interferometry has 20 stationary phases (Figure 2c). Locations of the stationary points are distributed at variety of points along the circle (Figure 3b). For all the points, azimuthal angles (ψ) are either 0 (for points a) or π (for points b).

DISCUSSION AND CONCLUSIONS

For seismic interferometry and ambient-noise correlation, spectral normalization has been often used to stabilize the calculation. Such normalizations, however, produce pseudo waves especially in later time in addition to the direct and scattered waves that are explained physically. With the stationary-phase approximation, I characterize all pseudo waves in deconvolution and crosscoherence interferometry. Because all stationary points can be estimated, potentially we will be able to extract information outside of the receivers; for example for term $\mathcal{T}_5$ (Figure 3a), the structural information along $\mathbf{r}_{2B-A}$ can be extracted. In addition, because amplitudes of each term are also revealed by this stationary-phase analysis, potentially we can extract attenuation. Importantly, measurements of time-lapse changes using coda waves of ambient-noise correlation can be biased by such pseudo waves.